ChemComm

COMMUNICATION

View Article Online
View Journal | View Issue

Cite this: *Chem. Commun.*, 2020, **56**, 619

Received 22nd September 2019,
Accepted 6th December 2019

DOI: 10.1039/c9cc07447c

rsc.li/chemcomm

A highly Li^+-conductive $HfNb_{24}O_{62}$ anode material for superior Li^+ storage†

Qingfeng Fu,[ab] Haijie Cao,[a] Guisheng Liang,[b] Lijie Luo,[b] Yongjun Chen,[b] Vignesh Murugadoss,[cde] Shide Wu,[cf] Tao Ding,[g] Chunfu Lin*[ab] and Zhanhu Guo*[c]

Highly Li^+-conductive $HfNb_{24}O_{62}$ is explored as a new intercalation-type niobium-based oxide anode material for superior Li^+ storage. $HfNb_{24}O_{62}$ owns a Wadsley–Roth shear structure with a large unit-cell volume, leading to a large Li^+ diffusion coefficient. $HfNb_{24}O_{62}$ shows a large capacity, safe operating potential, high rate performance and good cyclability.

Safe lithium-ion batteries (LIBs) with high power and energy density for electric vehicles (EVs) and hybrid electric vehicles (HEVs) have attracted intense attention.[1] However, the traditional graphite anode material is limited in such applications due to its low kinetics and unsafe lithiation potential.[2] As a promising substitute for graphite, $Li_4Ti_5O_{12}$ is appealing due to its safe operating potential (~1.57 V) and high rate performance after proper modifications.[3] However, the small theoretical capacity of $Li_4Ti_5O_{12}$ (175 mA h g^{-1}) has limited its large-scale applications. Therefore, new anode materials for safe, high-power and high-energy LIBs have been pursued.

In recent years, intercalation-type niobium-based oxides, such as $Ti_2Nb_{2x}O_{4+5x}$ (x = 2, 5 and 24),[4–11] $MNb_{11}O_{29}$ (M = Al, Cr, Fe and Ga),[12–15] and $W_5Nb_{16}O_{55}$,[16] have been developed as potential candidates to replace $Li_4Ti_5O_{12}$ due to their comparably safe operating potentials and much larger theoretical/practical capacities. Niobium is an appealing redox center in electrode materials because of its safe potential window in the range of 1.0–2.0 V for the redox couples of Nb^{4+}/Nb^{5+} and Nb^{3+}/Nb^{4+}, which can avoid the formation of dangerous lithium dendrites.[4] In light of multivalent properties, niobium-based oxides can deliver large theoretical capacities of 374–416 mA h g^{-1}, which are close to that of graphite and significantly surpass that of $Li_4Ti_5O_{12}$. In addition, with reported open Wadsley–Roth shear crystal structures consisting of 96–100% MO_6 octahedra and 0–4% MO_4 tetrahedra,[4] niobium-based oxides have been identified as typical intercalation-pseudocapacitive materials, which are beneficial for the capacity and fast-charging property. Despite such attractive features, niobium-based oxide anodes still show poor rate performance due to their intrinsically low Li^+ conductivities. Therefore, developing new niobium-based oxide anode materials with high Li^+ conductivities, Li^+-storage capacities, rate performance, and long-term stability is essential.

In this study, $HfNb_{24}O_{62}$ was synthesized by a facile and cost-effective solid-state reaction, and applied as a novel niobium-based oxide anode material with a high Li^+ conductivity to boost the Li^+ storage. In octahedral coordination, the Hf^{4+} ionic radius (0.710 Å) is larger than those of Ti^{4+} (0.605 Å), Al^{3+} (0.535 Å), Cr^{3+} (0.615 Å), Fe^{3+} (0.550 Å), Ga^{3+} (0.620 Å) and W^{6+} (0.600),[17] leading to increased lattice constants and unit-cell volume in $HfNb_{24}O_{62}$. A larger unit-cell volume usually corresponds to faster Li^+ diffusivity, benefiting the Li^+ transport kinetics.[18] Moreover, $HfNb_{24}O_{62}$ exhibits a monoclinic Wadsley–Roth shear crystal structure (space group of $C2$) consisting of 96% edge-sharing $(Hf,Nb)O_6$ octahedra linked by 4% $(Hf,Nb)O_4$ tetrahedra, in which Hf^{4+} and Nb^{5+} are disorder located. This three-dimensional skeleton bestows fast Li^+ diffusivity and high structural stability, guaranteeing fast lithiation/delithiation and excellent cyclability. Both the $HfNb_{24}O_{62}$/Li half-cell and $LiNi_{0.5}Mn_{1.5}O_4$//$HfNb_{24}O_{62}$ full-cell exhibit superior electrochemical properties for fast-charging, large-capacity, safe and durable Li^+ storage.

The detailed crystal structure of the as-prepared $HfNb_{24}O_{62}$ material was studied by XRD and a Rietveld refinement of the XRD pattern (Fig. 1a).[19] The characteristic peaks of $HfNb_{24}O_{62}$

[a] *Institute of Materials for Energy and Environment, School of Materials Science and Engineering, Qingdao University, Qingdao 266071, China. E-mail: linchunfu@qdu.edu.cn*
[b] *School of Materials Science and Engineering, Hainan University, Haikou 570228, China*
[c] *Integrated Composites Laboratory (ICL), Department of Chemical and Biomolecular Engineering, University of Tennessee, Knoxville, TN 37996, USA. E-mail: zguo10@utk.edu*
[d] *Key Laboratory of Materials Processing and Mold (Zhengzhou University), Ministry of Education, National Engineering Research Center for Advanced Polymer Processing Technology, Zhengzhou University, Zhengzhou 450002, China*
[e] *College of Chemical and Environmental Engineering, Shandong University of Science and Technology, Qingdao 266590, China*
[f] *Henan Provincial Key Laboratory of Surface and Interface Science, Zhengzhou University of Light Industry, Zhengzhou 450001, China*
[g] *College of Chemistry and Chemical Engineering, Henan University, Kaifeng 475004, China*

† Electronic supplementary information (ESI) available. See DOI: 10.1039/c9cc07447c

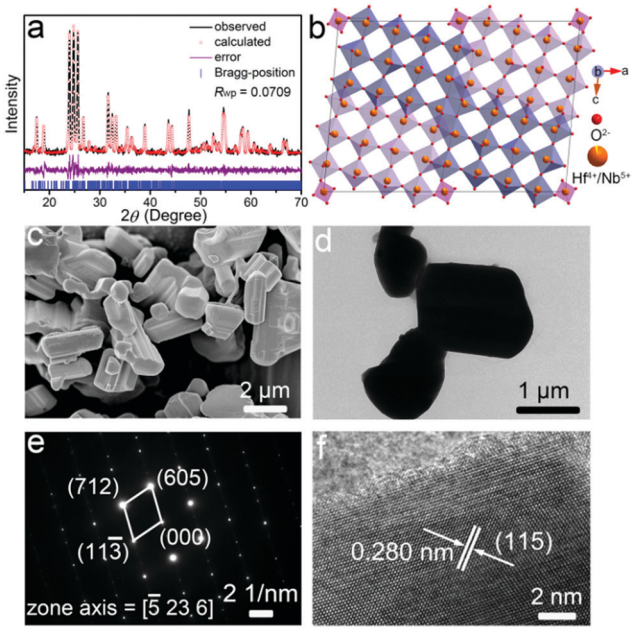

Fig. 1 (a) XRD pattern, (b) crystal structure, (c) FESEM image, (d) TEM image, (e) SAED pattern, and (f) HRTEM image of $HfNb_{24}O_{62}$. R_{wp}: weighted profile residual.

are consistent with those of $TiNb_{24}O_{62}$ (space group of $C2$).[6] $HfNb_{24}O_{62}$ owns a robust crystal structure, with the structural unit having a 3 × 4 (Hf,Nb)O_6 octahedron-block and a half (Hf,Nb)O_4 tetrahedron at the block corner (Fig. 1b). The lattice parameters were Rietveld-refined to be a = 29.92508(125) Å, b = 3.82525(14) Å, c = 21.21133(87) Å, β = 95.068(5)°, and V = 2418.588(167) Å^3. Detailed lattice parameters are given in Table S1 (ESI†). Due to the larger Hf^{4+} (0.710 Å) ionic radius than Ti^{4+} (0.605 Å), the unit-cell volume of $HfNb_{24}O_{62}$ is larger than that of $TiNb_{24}O_{62}$,[6] which implies wider Li^+ transport pathways in the $HfNb_{24}O_{62}$ lattice. The survey XPS spectrum of $HfNb_{24}O_{62}$ reveals the presence of Hf, Nb, O and C (reference) elements (Fig. S1a, ESI†). The detailed Hf-4f (Fig. S1b, ESI†) and Nb-3d (Fig. S1c, ESI†) spectra indicate that the Hf and Nb valence states are +4 and +5,[4,20] respectively.

The FESEM (Fig. 1c) and TEM (Fig. 1d) images reveal that the $HfNb_{24}O_{62}$ material is composed of irregular and dense particles with particle sizes varying from ~2 to ~10 μm, giving a low specific surface area of 0.38 m^2 g^{-1} (Fig. S2, ESI†). The corresponding SAED pattern in Fig. 1e confirms high crystallinity and reveals a single-crystalline feature of the $HfNb_{24}O_{62}$ primary particles. An interplanar spacing of 0.280 nm measured from the HRTEM image (Fig. 1f) corresponds to the (115) crystallographic plane of $HfNb_{24}O_{62}$. Besides, the EDX mappings (Fig. S3, ESI†) indicate that the Nb, O and Hf elements are well-dispersed in the whole microparticle, verifying the formation of pure $HfNb_{24}O_{62}$.

The electrochemical properties of $HfNb_{24}O_{62}$ were mainly studied using half-cells. Fig. 2a shows the CV curves of the $HfNb_{24}O_{62}$/Li cell for the initial four cycles at a sweep rate of 0.2 mV s^{-1}. The difference in the discharge portion of the first CV curve from the subsequent cycles is likely due to the incomplete Li^+ extraction from the $HfNb_{24}O_{62}$ lattice in the first cycle.[21] After the first cycle, the peak positions and corresponding currents are very stable, suggesting good electrochemical reversibility and cyclability of $HfNb_{24}O_{62}$. In the subsequent sweeps, two highly overlapping CV peak pairs located at ~2.0/~2.0 and 1.77/1.55 V were assigned to the reversible transformation for the redox couple of Nb^{4+}/Nb^{5+}. The shoulder peaks located at 1.34/1.14 V correspond to the redox couple of Nb^{3+}/Nb^{4+}.[12] Consequently, the estimated $HfNb_{24}O_{62}$ mean operating potential (~1.66 V) based on the intermediate potential of two intensive peaks at 1.77/1.55 V is close to those of $Li_4Ti_5O_{12}$ (~1.57 V),[3] $TiNb_2O_7$ (~1.64 V),[5] $TiNb_{24}O_{62}$ (~1.66 V)[6] and $Ti_2Nb_{10}O_{29}$ (~1.70 V).[11] Such a reasonably high operating potential of $HfNb_{24}O_{62}$ indicates its high safety performance.

Fig. 2b displays the initial three-cycle discharging/charging curves of the $HfNb_{24}O_{62}$/Li cell recorded at 0.1C. The observed typical potential plateau at ~1.66 V in the discharging/charging curves resulted from a double-phase transformation reaction. The sloping regions at 3.0–1.67 and 1.65–0.8 V were assigned to two different solid–solution reactions.[8] $HfNb_{24}O_{62}$ shows an initial Coulombic efficiency of 93.8% and large reversible capacity of 272 mA h g^{-1} at 0.1C. This practical capacity of $HfNb_{24}O_{62}$ is >100 mA h g^{-1} larger than that of $Li_4Ti_5O_{12}$ and surpasses the majority of the reported intercalation-type niobium-based oxide anode materials (Fig. 2c).[3,4,6,9,10,14–16,22,23] The high initial Coulombic efficiency can be due to the fact that little SEI layers formed on the $HfNb_{24}O_{62}$ particle surfaces above 0.8 V.

The rate performance of $HfNb_{24}O_{62}$ was investigated at various current rates for every ten cycles, as shown in Fig. 2d and e. $HfNb_{24}O_{62}$ delivers large reversible capacities of 223, 195, 174, 138 and 105 mA h g^{-1} at 0.5, 1, 2, 5 and 10C, respectively. When the current rate gradually returns from 10C to 0.5C, the capacity is recovered to its original value. When cycled at 1C, $HfNb_{24}O_{62}$ shows a small capacity change from 193 to 182 mA h g^{-1} after 100 cycles, giving 94.3% capacity retention (Fig. 2f and Fig. S4, ESI†). When cycled at 10C, $HfNb_{24}O_{62}$ shows 87.1% capacity retention even after 500 cycles during the prolonged cycling (Fig. 2g and Fig. S5, ESI†). Such superior cyclability can be due to the stable crystal structure and good Li^+-transport kinetics of $HfNb_{24}O_{62}$.

To interpret the high rate performance of $HfNb_{24}O_{62}$, its Li^+-storage kinetics was analyzed by additional CV experiments recorded at different sweep rates (Fig. 2h). It was found that the cathodic/anodic CV peak current exhibited power law dependence on the sweep rate with an exponent of 0.67/0.74 (Fig. 2i),[7,24] suggesting that the pseudocapacitive behaviour significantly contributed to the fast charge storage of $HfNb_{24}O_{62}$ since it is well known that exponents of 0.5 and 1 indicate diffusion-controlled and pseudocapacitive charge storage, respectively.

A galvanostatic intermittent titration technique (GITT) with a current pulse at 0.1C for 10 min between rest intervals for 20 min was applied to elucidate the Li^+ diffusion coefficient (D_{Li}) of $HfNb_{24}O_{62}$ during the initial two cycles. Based on Fick's second law (see ESI†),[25] the evolving D_{Li} of $HfNb_{24}O_{62}$ at each potential in the discharging (lithiation) and charging (delithiation) processes is determined and plotted in Fig. 2j. The D_{Li} values show

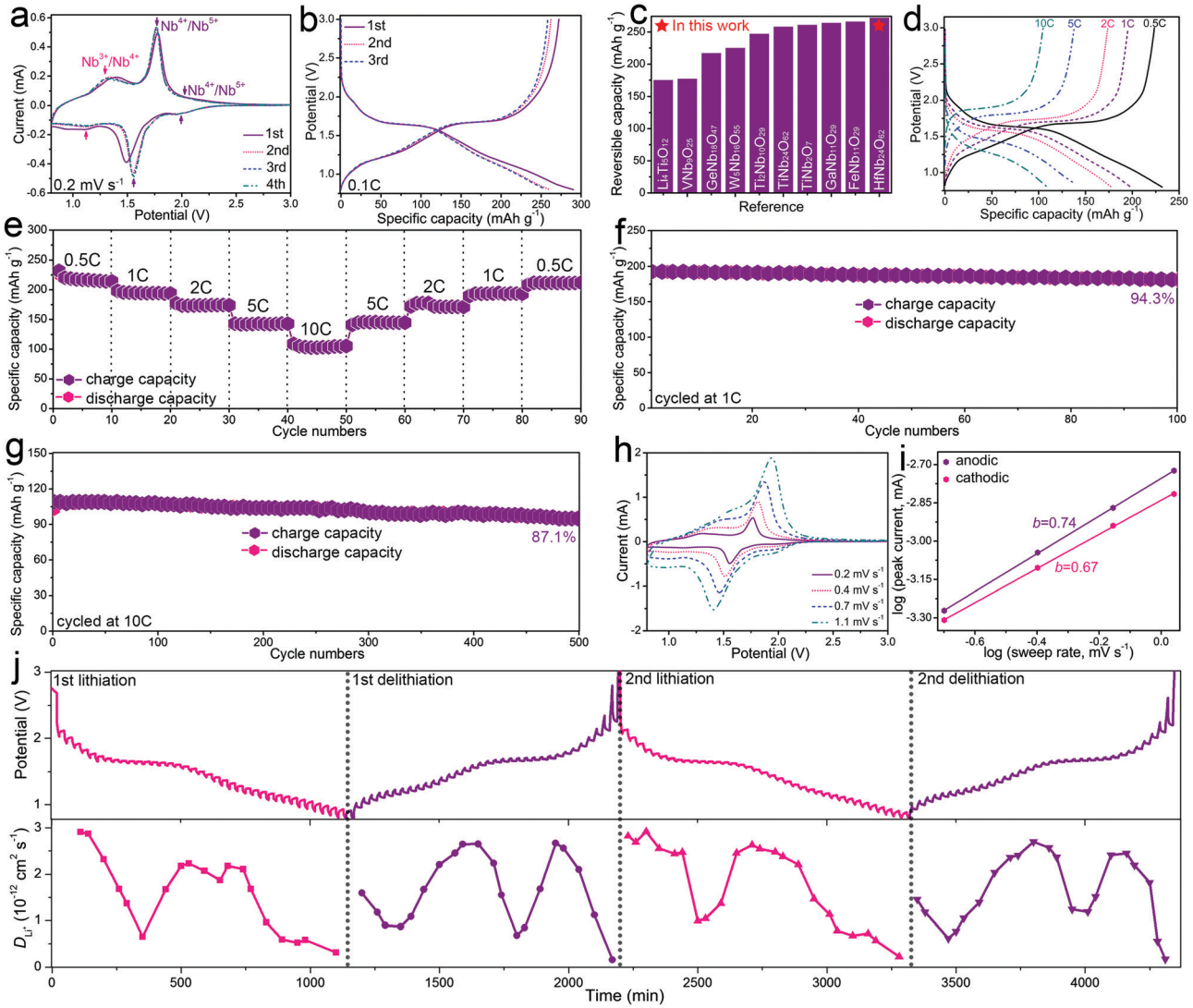

Fig. 2 Electrochemical characterizations of the $HfNb_{24}O_{62}$/Li cell: (a) CVs at 0.2 mV s^{-1}, (b) discharging/charging curves at 0.1C, (c) comparisons of reversible capacity of $HfNb_{24}O_{62}$ with other intercalation-type oxide anode materials, (d) discharging/charging curves at different current rates, (e) rate performance, cyclability at (f) 1C and (g) 10C, (h) CVs at different sweeping rates, (i) exponential relationship between CV peak current and sweep rate, and (j) GITT curves and corresponding Li^+ diffusion coefficients (initial two cycles).

a similar variation trend in the two cycles, and minor values appear in the plateau region (~1.7 V), where the Li^+ interaction with the host matrix is strong during the two-phase transition reaction. During the first lithiation/delithiation processes, the D_{Li} value varies from 1.51×10^{-13} to 2.91×10^{-12} cm^2 s^{-1}, averaging at 1.61×10^{-12} cm^2 s^{-1}. The average D_{Li} value in the second lithiation/delithiation processes (1.70×10^{-12} cm^2 s^{-1}) is slightly larger than that of the initial cycle, but the curves are similar to those in the initial cycle. It is noteworthy that the Li^+ diffusion coefficient of $HfNb_{24}O_{62}$ is significantly larger than those of the reported niobium-based oxide anode materials (Table S2, ESI†), which can be ascribed to its open Wadsley–Roth shear crystal structure with an enlarged unit-cell volume. Clearly, the fast Li^+ diffusivity together with the significant pseudocapacitive behaviour of $HfNb_{24}O_{62}$ greatly contributes to its superior Li^+ storage (especially its rate performance).

To demonstrate the practical application of $HfNb_{24}O_{62}$, a full cell with a $HfNb_{24}O_{62}$ anode and a $LiNi_{0.5}Mn_{1.5}O_4$ cathode was fabricated (Fig. 3a). The $LiNi_{0.5}Mn_{1.5}O_4$//$HfNb_{24}O_{62}$ full cell affords a large charge capacity of 213 mA h g^{-1} with an average operating voltage of ~3.0 V at 0.1C (Fig. 3b). This high voltage agrees with the CV result (Fig. 3c). As the current rate gradually increases to 0.5, 1, 2, 5 and even 10C, the reversible capacity retains 143, 130, 116, 95 and 78 mA h g^{-1}, respectively (Fig. 3d). When the current rate returns from 10C to 0.5C, the obtained capacity of 141 mA h g^{-1} indicates good electrochemical reversibility (Fig. 3e). The full cell also presents outstanding cyclability at both 1C (83.4% capacity retention after 100 cycles, Fig. 3f) and 5C (84.7% capacity retention after 500 cycles, Fig. 3g). The full cell can power a green light-emitting diode (LED) after being cycled 500 times at 5C (Fig. 3g inset).

In summary, highly-Li^+-conductive $HfNb_{24}O_{62}$ is demonstrated as a novel anode material to realize superior Li^+ storage.

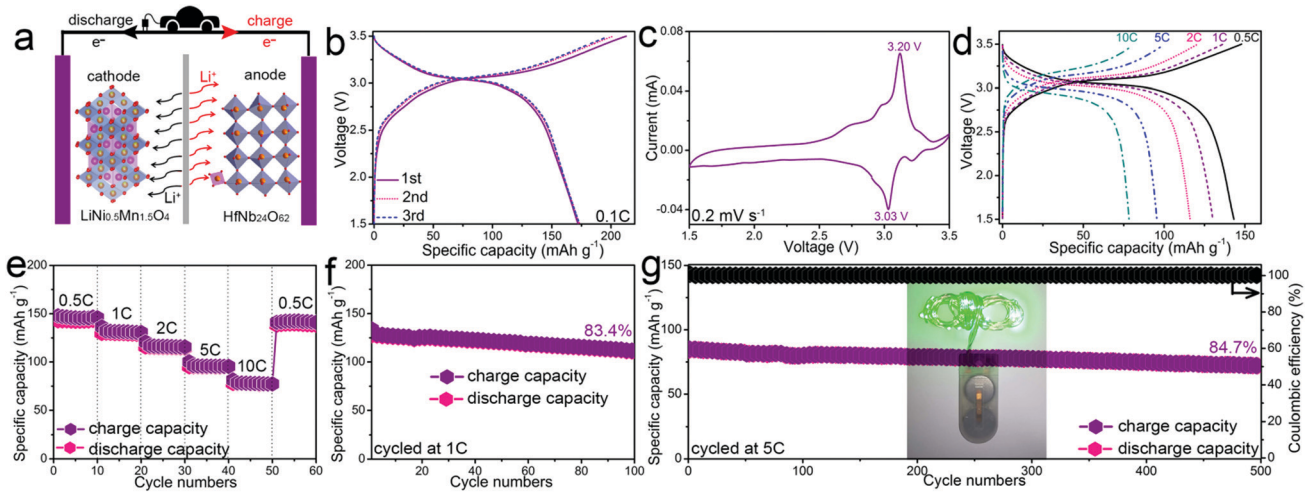

Fig. 3 (a) Schematic illustration of the $LiNi_{0.5}Mn_{1.5}O_4$//$HfNb_{24}O_{62}$ full cell. Electrochemical characterizations of the $LiNi_{0.5}Mn_{1.5}O_4$//$HfNb_{24}O_{62}$ full cell: (b) initial three-cycle charging/discharging curves at 0.1C, (c) CV at 0.2 mV s^{-1}, (d) charging/discharging curves at different current rates, (e) rate performance, and cyclability at (f) 1C and (g) 5C (inset: green LED lit up by the full cell).

Both the open Wadsley–Roth shear crystal structure and enlarged unit-cell volume lead to favorable Li^+ conduction. Benefiting from the robust host framework and fast ion diffusion pathways, $HfNb_{24}O_{62}$ exhibits prominent electrochemical properties. At 0.1C, it displays a large capacity of 272 mA h g^{-1} with a relatively safe operating potential of ~1.66 V and a high initial Coulombic efficiency of 93.8%. Even at 10C, a remarkable reversible capacity of 105 mA h g^{-1} is preserved. Furthermore, it exhibits good long-term cyclability, as indicated by 87.1% capacity retention after 500 cycles at 10C. More importantly, a $LiNi_{0.5}Mn_{1.5}O_4$//$HfNb_{24}O_{62}$ full cell also exhibits high rate performance with 213 mA h g^{-1} at 0.1C and 78 mA h g^{-1} at 10C, and good long-term cyclability with 84.7% capacity retention after 500 cycles at 5C. This work can benefit the future designs of highly-Li^+-conductive and fast-charging electrode materials.

This work was supported by the National Natural Science Foundation of China (51762014) and China Postdoctoral Science Foundation (2019M652316).

Conflicts of interest

There are no conflicts to declare.

Notes and references

1 (*a*) H. T. Sun, L. Mei and J. F. Liang, *et al.*, *Science*, 2017, **356**, 599; (*b*) Y. Zhang, Y. An and L. Wu, *et al.*, *J. Mater. Chem. A*, 2019, **7**, 19668; (*c*) C. Hou, J. Wang and W. Du, *et al.*, *J. Mater. Chem. A*, 2019, **7**, 13460.
2 (*a*) S. R. Sivakkumar, J. Y. Nerkar and A. G. Pandolfo, *Electrochim. Acta*, 2010, **55**, 3330; (*b*) M. Idrees, S. Batool and J. Kong, *et al.*, *Electrochim. Acta*, 2019, **296**, 925; (*c*) R. Li, C. Lin and N. Wang, *et al.*, *Adv. Compos. Hybrid Mater.*, 2018, **1**, 440.
3 (*a*) C. F. Lin, X. Y. Fan, Y. L. Xin, F. Q. Cheng, M. O. Lai, H. H. Zhou and L. Lu, *J. Mater. Chem. A*, 2014, **2**, 9982; (*b*) M. Idrees, L. Liu and S. Batool, *et al.*, *Eng. Sci.*, 2019, **6**, 64.
4 L. Hu, L. J. Luo, C. F. Lin, R. J. Li and Y. J. Chen, *J. Mater. Chem. A*, 2018, **6**, 9799.
5 C. F. Lin, S. Yu, S. Q. Wu, S. W. Lin, Z. Z. Zhu, J. B. Li and L. Lu, *J. Mater. Chem. A*, 2015, **3**, 8627.
6 C. Yang, S. J. Deng, C. F. Lin, S. W. Lin, Y. J. Chen, J. B. Li and H. Wu, *Nanoscale*, 2016, **8**, 18792.
7 S. F. Lou, X. Q. Cheng and Y. Zhao, *et al.*, *Nano Energy*, 2017, **34**, 15.
8 X. Y. Wu, J. Miao, W. Z. Han, Y. S. Hu, D. F. Chen, J. Lee, J. Kim and L. Q. Chen, *Electrochem. Commun.*, 2012, **25**, 39.
9 J. L. Gao, X. Q. Cheng, S. F. Lou, Y. L. Ma, P. J. Zuo, C. Y. Du, Y. Z. Gao and G. P. Yin, *J. Alloys Compd.*, 2017, **728**, 534.
10 W. L. Wang, B. Oh, J. Park, H. Ki, J. Jang, G. Lee, H. Hu and M. Ham, *J. Power Sources*, 2015, **300**, 272.
11 C. F. Lin, S. Yu, H. Zhao, S. Q. Wu, G. Z. Wang, L. Yu, Y. F. Li, Z. Z. Zhu, J. B. Li and S. W. Lin, *Sci. Rep.*, 2015, **5**, 17836.
12 R. T. Zheng, S. S. Qian, X. Cheng, H. X. Yu, N. Peng, T. T. Liu, J. D. Zhang, M. T. Xia, H. J. Zhu and J. Shu, *Nano Energy*, 2019, **58**, 399.
13 Q. F. Fu, X. Liu, J. R. Hou, Y. R. Pu, C. F. Lin, L. Yang, X. Z. Zhu, L. Hu, S. W. Lin, L. J. Luo and Y. J. Chen, *J. Power Sources*, 2018, **397**, 231.
14 X. M. Lou, C. F. Lin, Q. Luo, J. B. Zhao, B. Wang, J. B. Li, Q. Shao, X. K. Guo, N. Wang and Z. H. Guo, *ChemElectroChem*, 2017, **4**, 3171.
15 X. M. Lou, Q. F. Fu, J. Xu, X. Liu, C. F. Lin, J. X. Han, Y. P. Luo, Y. J. Chen, X. Y. Fan and J. B. Li, *ACS Appl. Nano Mater.*, 2018, **1**, 183.
16 K. J. Griffith, K. M. Wiaderek, G. Cibin, L. E. Marbella and C. P. Grey, *Nature*, 2018, **559**, 556.
17 R. D. Shannon, *Acta Crystallogr., Sect. A: Found. Crystallogr.*, 1976, **32**, 751.
18 Y. Wang, W. D. Richards, S. P. Ong, L. J. Miara, J. C. Kim, Y. Mo and G. Ceder, *Nat. Mater.*, 2015, **14**, 1026.
19 B. H. Toby, *J. Appl. Crystallogr.*, 2001, **34**, 210.
20 A. N. Mansour, *Surf. Sci. Spectra*, 1994, **3**, 221.
21 X. Lu, Z. L. Jian, Z. Fang, L. Gu, Y. S. Hu, W. Chen, Z. X. Wang and L. Q. Chen, *Energy Environ. Sci.*, 2011, **4**, 2638.
22 F. M. Ran, X. Cheng, H. X. Yu, R. T. Zheng, T. T. Liu, X. F. Li, N. Ren, M. Shui and J. Shu, *Electrochim. Acta*, 2018, **282**, 634.
23 G. Li, X. L. Wang and X. M. Ma, *J. Mater. Chem. A*, 2013, **1**, 12409.
24 J. P. Yue, C. Suchomski and P. Voepel, *et al.*, *J. Mater. Chem. A*, 2017, **5**, 1978.
25 W. Weppner and R. A. Huggins, *J. Electrochem. Soc.*, 1977, **124**, 1569.

